# Supporting Information

# The construction of alkynyl-containing porous polymer for enhanced photocatalytic $H_2O_2$ generation

*Yumiao Wang [a, #], Wenwen Chi [a, #], Renbao Zhang [a], Yingxin Guo [a], Xinyu Sun [a], Hui Zhao [a], Jiawei Zhang [a], Yuming Dong [a, *] and Yongfa Zhu [b]*

[a]International Joint Research Center for Photoresponsive Molecules and Materials, Key Laboratory of Synthetic and Biological Colloids, School of Chemical and Material Engineering, Jiangnan University, Wuxi 214122, China.

[b] Department of Chemistry, Tsinghua University, Beijing 100084, China

[*] Corresponding authors: Prof. Yuming Dong, dongym@jiangnan.edu.cn

[#] These authors contributed equally: Yumiao Wang and Wenwen Chi

## General Information

### Experimental section

### Details in measurements

### Determination of apparent quantum yield (AQY)

The photocatalytic reaction was carried out with 100 mg photocatalyst in 40 ml water in a borosilicate glass bottle by 300 W Xe lamp irradiation equipped with a quartz optical fibre. The bottle was kept at 70 °C in oil bath and bubbling with $O_2$ during the reaction and irradiated for 30 mins with magnetic stirring. The incident light was filtered with a bandpass filter (400 ± 10 nm, 420

± 10 nm, 500 ± 10 nm, 550 ± 10 nm, 600 ± 10 nm). The photon number entered into the reaction bottle was determined with a UV spectral illuminance meter.

$$\Phi AQY\ (\%) = 2N_{H2O2} / N_{photons} \times 100\%$$

**RDE measurements:**

A glassy carbon rotating disk electrode (PINE Research Instrumentation, USA) was served as the substrate for working electrode. The working electrode was prepared as follows: 20 mg of power photocatalysts was dispersed in 2 mL of ethanol containing 20 μL of Nafion by ultrasonication. 20 μL of the above slurry was put onto the disk electrode and dried at room temperature. The linear sweep voltammogram (LSV) curves were recorded in an Ar or $O_2$-saturated 0.1 M phosphate buffer solution (pH = 7) at room temperature and a scan rate of 10 mV $s^{-1}$ with different rotation speeds. The average number of electrons (n) was calculated by the Koutecky-Levich equation:

$$\frac{1}{J} = \frac{1}{J_L} + \frac{1}{J_K} + \frac{1}{B_w^{1/2}} + \frac{1}{J_K}$$

$$B = 0.62nFC_0D_0^{2/3}V^{-1/6}$$

where J is the current density, $J_K$ and $J_L$ are the kinetic and diffusion-limiting current densities, ω is the rotating speed (rpm), n is transferred electron number, F is Faraday constant (96485 C $mol^{-1}$), $C_0$ is the bulk concentration of $O_2$ ($1.26 \times 10^{-3}$ mol $cm^{-3}$), $D_0$ is the diffusion coefficient of $O_2$ ($2.7 \times 10^{-5}$ $cm^2$ $s^{-1}$), and *v* is kinetic viscosity of the electrolyte (0.01 $cm^2$ $s^{-1}$), respectively.

**RRDE measurements**

The rotating disk electrode (RRDE) was tested in $O_2$ saturated phosphate buffer solution (0.1 M, pH=6.9), with glassy carbon electrode as the working electrode, Pt ring as the counter electrode and Ag/AgCl electrode as the reference electrode. The potential of the Ag/AgCl reference electrode was converted to the potential of RHE according to the Nernst equation: E (vs.RHE) = E (vs. Ag/AgCl)

+ 0.0591 × pH + 0.197. The ring potential of the disk electrode was maintained at 1.45 V (vs RHE). The linear sweep voltammetry (LSV) tests were performed at the scan speed of 5 mV/s and revolutions of 800, 1000, 1200,1400 and 1600 rpm in an $O_2$-saturated electrolyte. The number of the transferred electrons was calculated following

$$Eq.(1): n = 4\frac{I_d}{I_d + {}^{I_r}/_{N}}$$

The selectivity of $H_2O_2$ was determined by

$$Eq.(2): H_2O_2\% = 200\frac{{}^{I_r}/_{N}}{I_d + {}^{I_r}/_{N}}$$

where Id is the disc current and Ir is the ring current. The collection efficiency (N) was determined to be 37%.

**Photocurrents and photoelectrochemical measurements**

The Mott-Schottky plots, photocurrent response, open circuit potentials and electrochemical impedance of the photocatalysts were measured on an electrochemical workstation (CHI660E, CHI Instruments, Shanghai, China). A 300 W Xe lamp was utilized as the light source and $Na_2SO_4$ (0.5 M) aqueous solution was used as the supporting electrolyte throughout the photocurrent measurements. A platinum wire and Ag/AgCl electrode were used as counter electrode and reference electrode. 100 μL of Nafion, dry ethanol (1.0 mL) and photocatalyst (5.0 mg) were sonicated for 30 min. Then 200 μL of the suspension was dripped onto an ITO glass substrate and dried. The application potential was converted to RHE potentials with respect to Ag/AgCl using the following equation

***In situ* DRIFTS Characterization**

*In situ* diffuse reflectance infrared Fourier transform spectroscopy (DRIFTS) measurements were performed using on a Nicolet iS50 spectrometer (Thermo, USA) using the KBr pellet technique. Fourier-transform spectrometer equipped with a Harrick diffuse reflectance accessory at the Infrared Spectroscopy. Each spectrum was recorded by averaging 64 scans at 8 cm-1 spectral resolution. The chamber was sealed with two ZnSe windows. The sample was prepared as follows: 10 mg of power photocatalysts was dispersed in 2 mL of ethanol containing 20 μL of Nafion by ultrasonication. 200 μL of the above slurry was put onto the disk and dried at room temperature.

**DFT calculation method**

Geometric optimization was performed using Gaussian 09 D.01 based on the B3LYP exchange-correlation generalized function, 6-31G(d) basis group and $H_2O$ as solvent model, and frequency calculations were also performed to ensure that there are no imaginary frequencies in the stable group states [1-8]. The adsorption energy of $O_2$ ($E_{ads}$ ($O_2$)) is calculated as follows:

$$E_{ads}(O_2) = E(*O_2) - E(*) - E(O_2)$$

where $E(*O_2)$ , $E(*)$ , $E(O_2)$ are the total energy of $O_2$ adsorbed on the sample surface, the energy of the original sample surface, and the energy of $O_2$, respectively

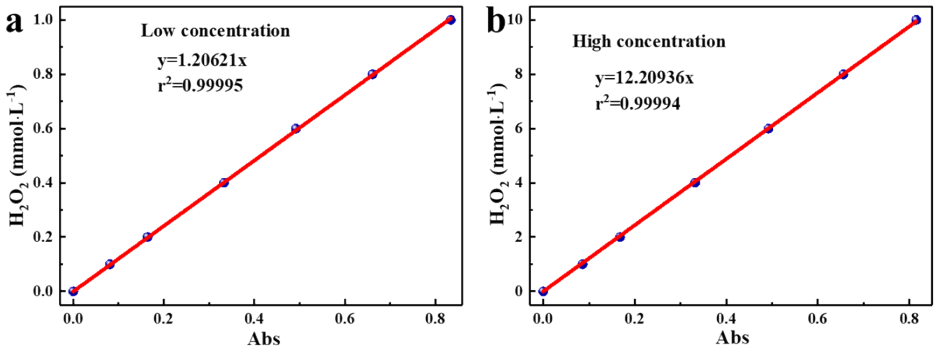


**Figure S1. (a) and (b) Correspond to the standard curves of low and high. concentrations of $H_2O_2$ calibrated by the iodination method, respectively**.

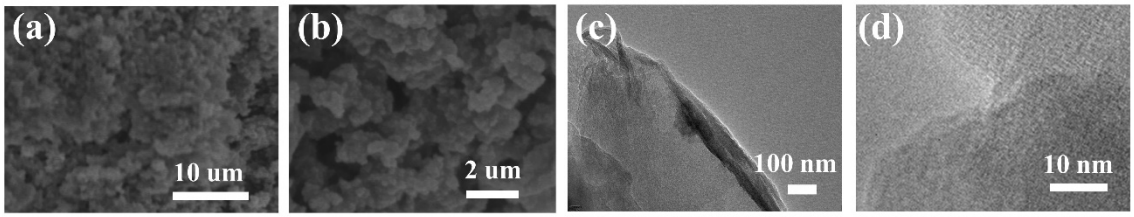


**Figure S2 (a) and (b) SEM images of POP-DF. (c) and (d) TEM images of POP-DF.**

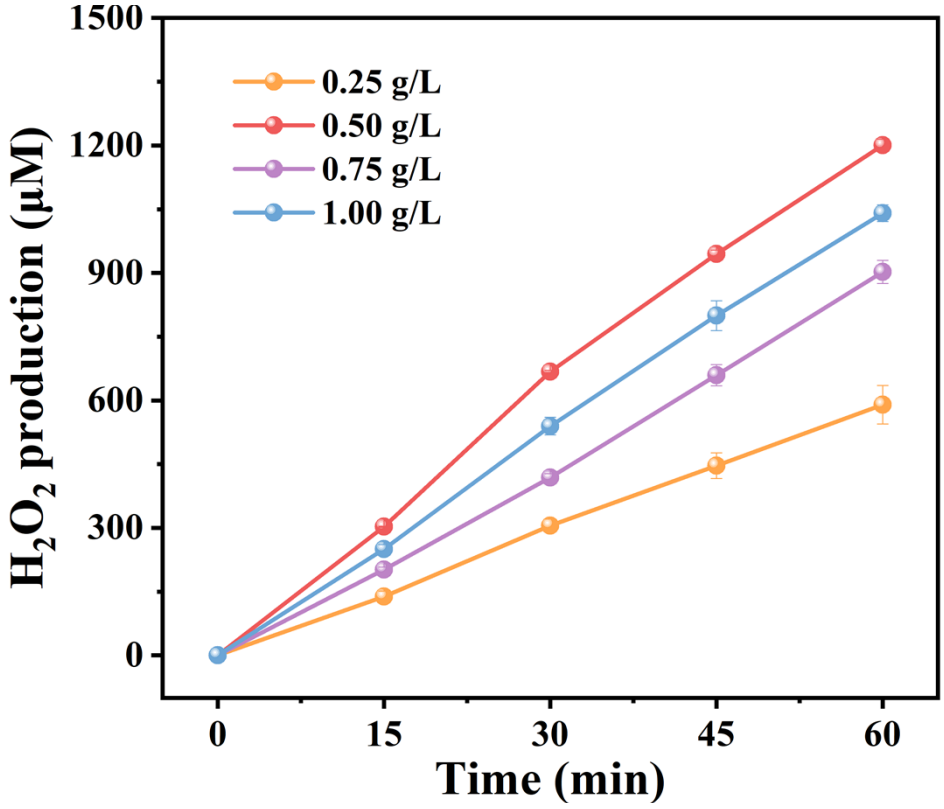


**Figure S3. Hydrogen peroxide production rate at different conditions of POP-DT.**

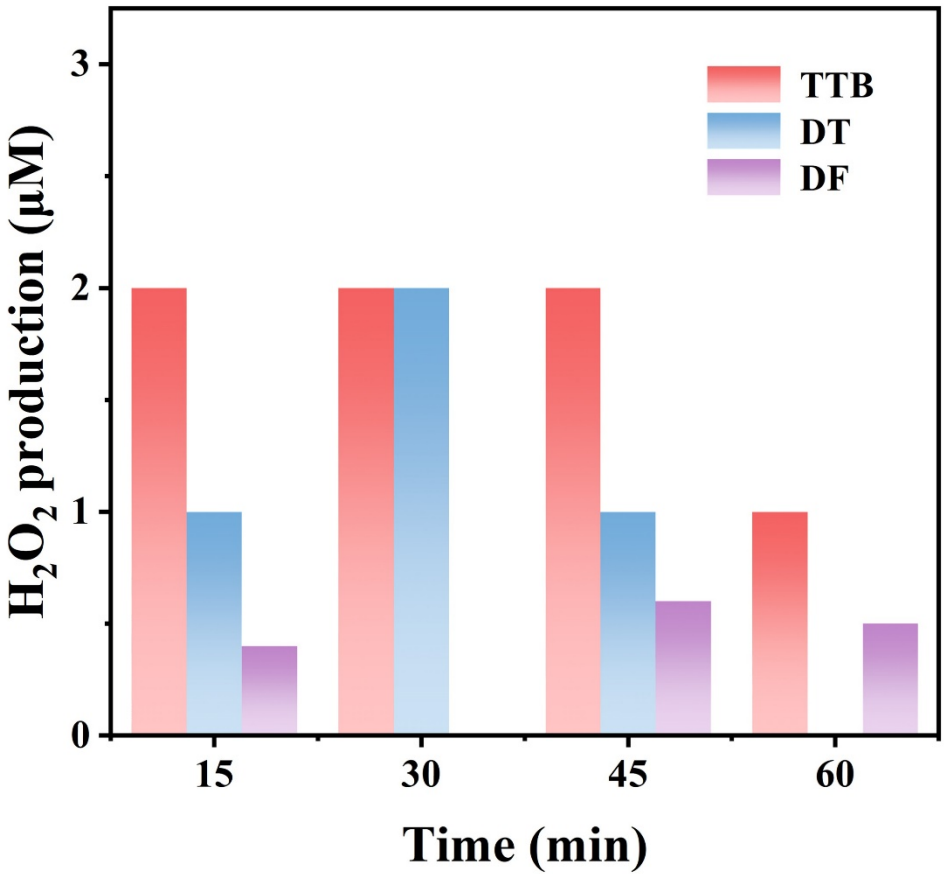


**Figure S4. Photocatalytic activity of corresponding monomer**.

According to the experimental results, none of the monomers used in the synthesis of POPs had photocatalytic hydrogen peroxide production effects.

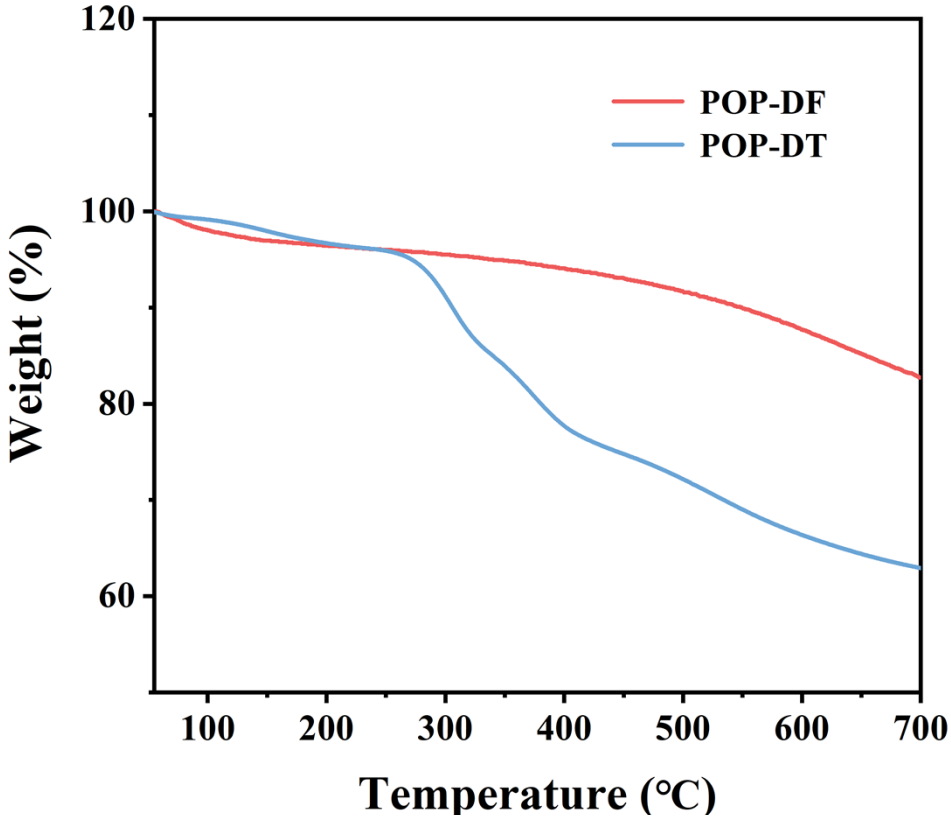


**Figure S5. TGA curves of POP-DT and POP-DF.**

**Table S1 Wavelength dependent AQE of photocatalytic $H_2O_2$ evolution over POP-DT.**

| Wavelength (nm) | 400 | 420 | 500 | 550 | 600 |
|---|---|---|---|---|---|
| Absorbance | 0.037 | 0.029 | 0.021 | 0.016 | 0.011 |
| Light intensity (mW $cm^{-2}$) | 5.4 | 6 | 6.3 | 6.5 | 6.8 |
| Irradiation area ($cm^2$) | 1 | 1 | 1 | 1 | 1 |
| Irradiation time (h) | 1 | 1 | 1 | 1 | 1 |
| Volume (mL) | 40 | 40 | 40 | 40 | 40 |
| AQY (%) | 2.67 | 1.79 | 1.04 | 0.70 | 0.42 |

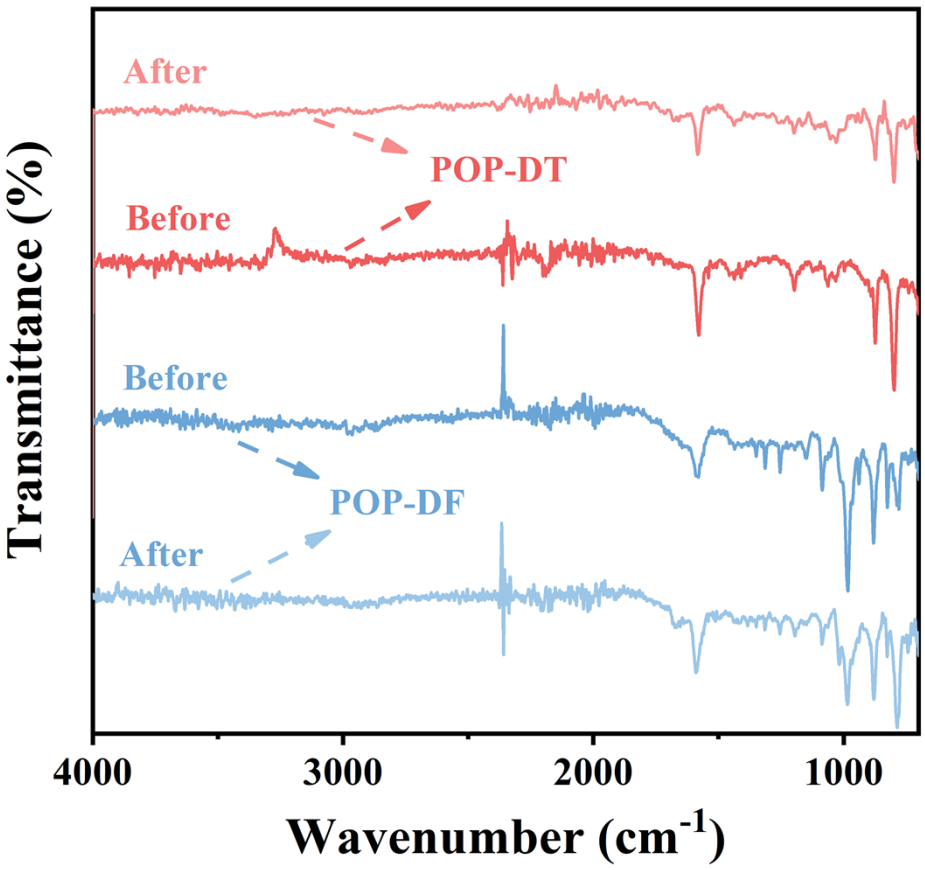


**Figure S6. The FTIR of POPs photocatalyst before and after photoreaction.**

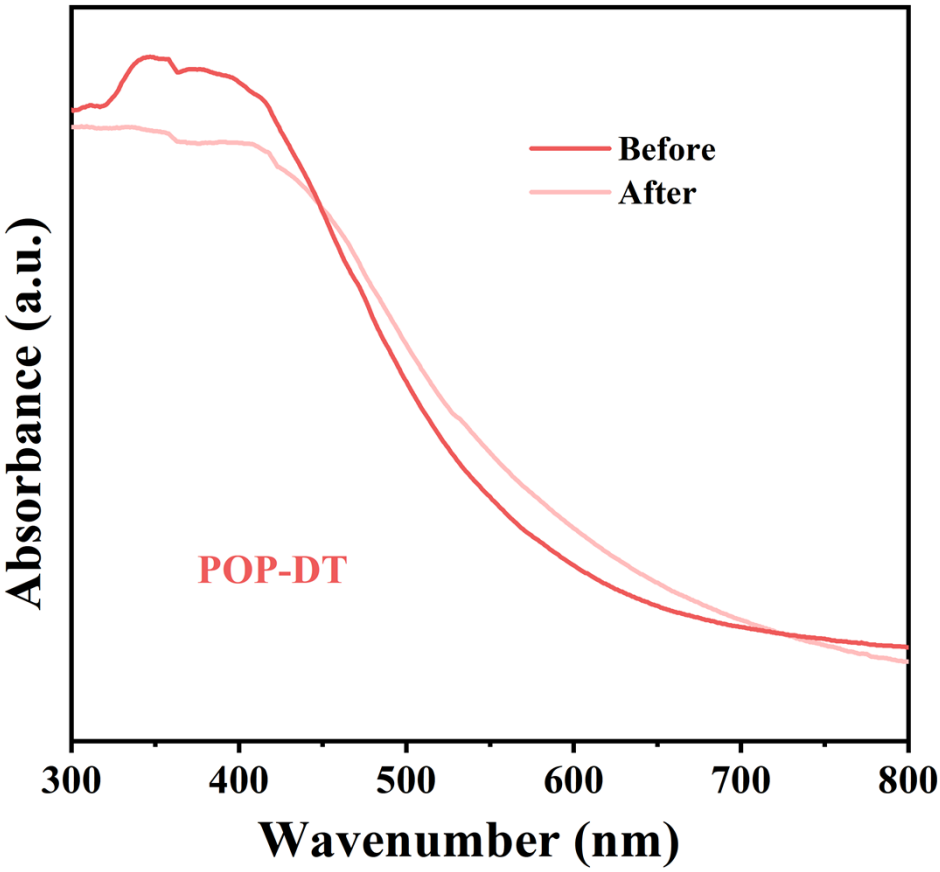


**Figure S7. The UV-vis of POP-DT before and after photoreaction.**

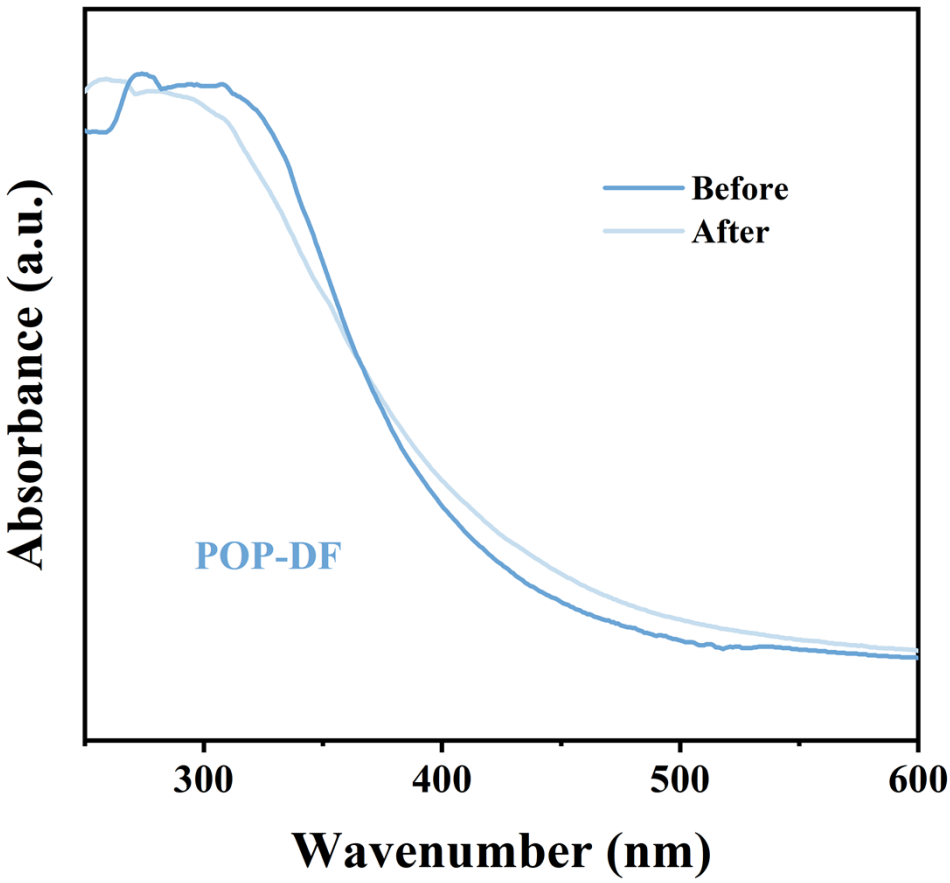


**Figure S8. The UV-vis of POP-DF before and after photoreaction.**

Through the test results, we can It was found that there was no significant change in the UV-vis absorption of POPs before and after illumination, which verified the stability of the POPs in this article.

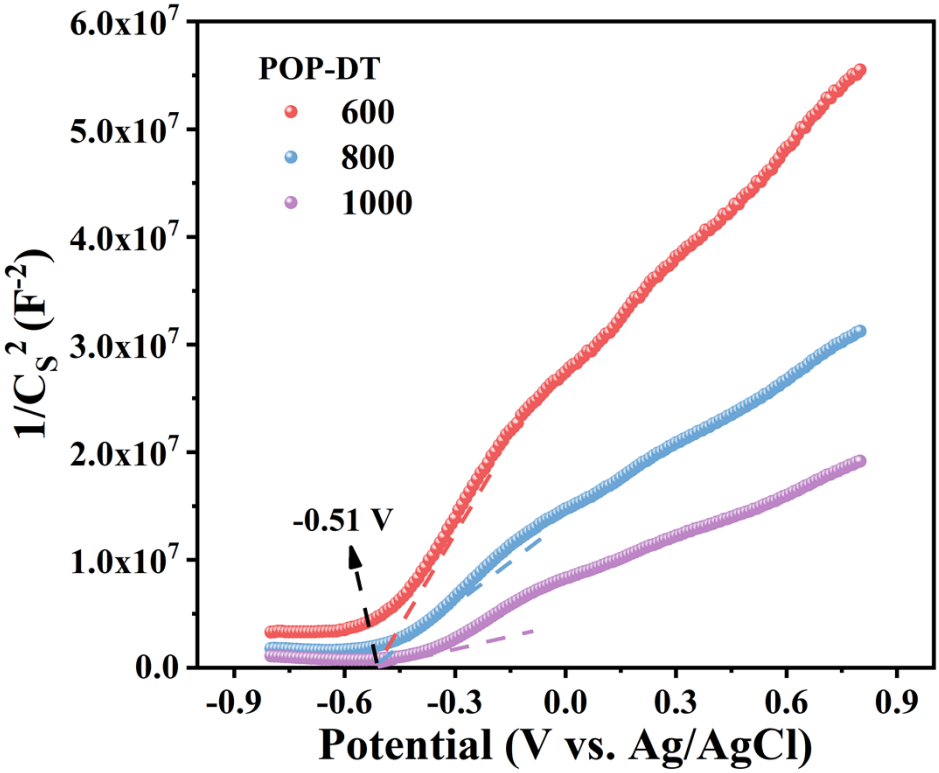


**Figure S9. Mott-Schottky plots of POP-DT at the isoelectric point**.

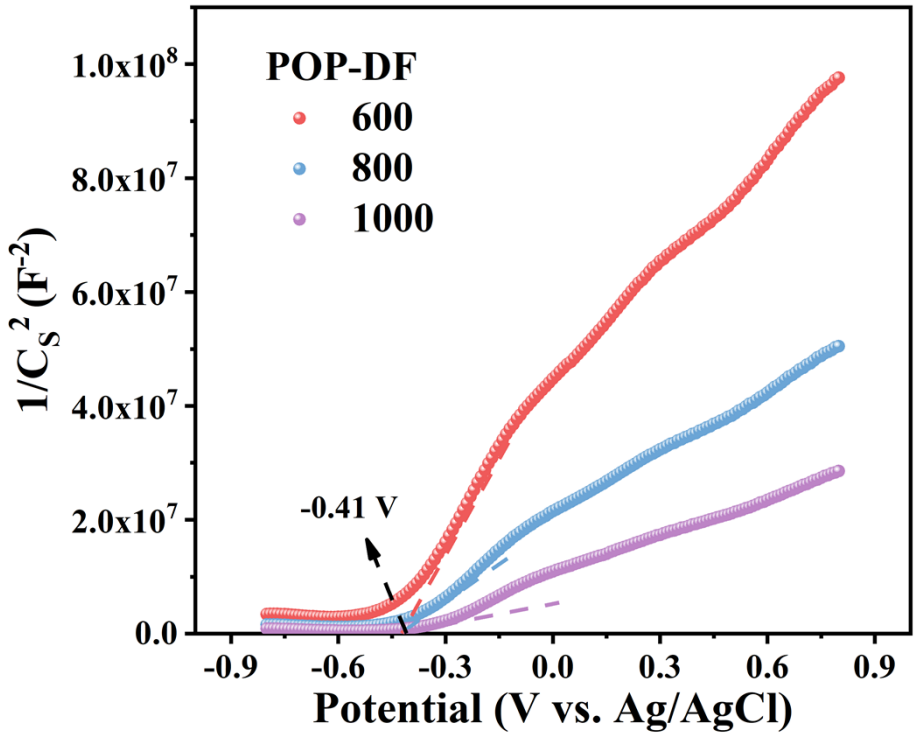


**Figure S10. Mott-Schottky plots of POP-DF at the isoelectric point**.

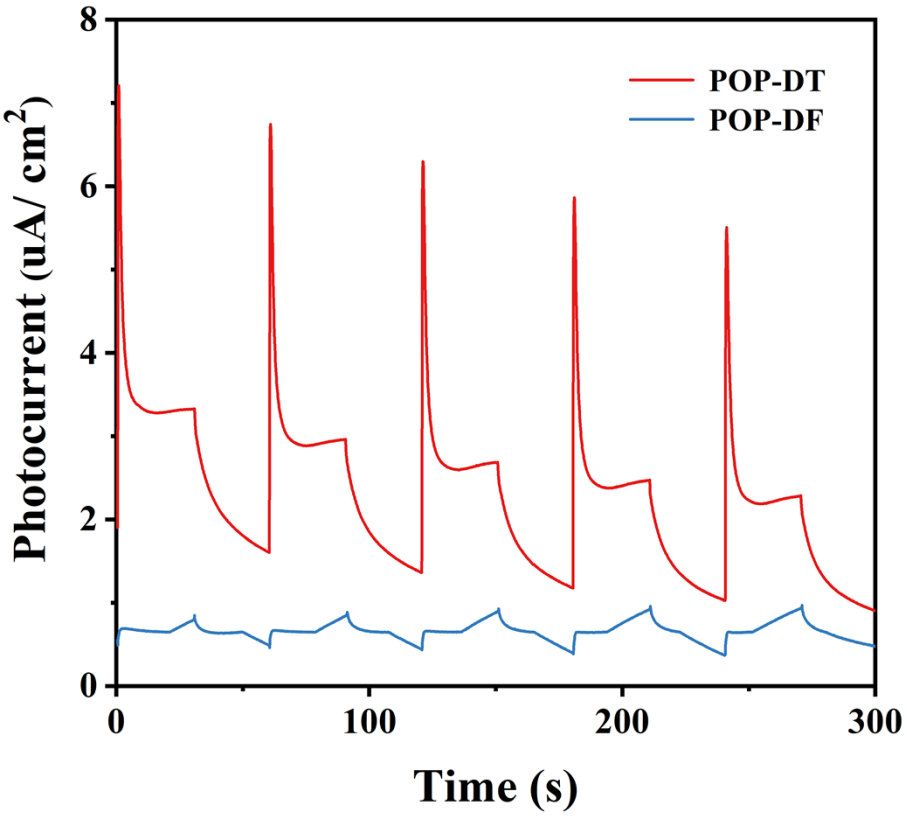


**Figure S11. I–t curves of POPs under visible light irradiation (λ>420 nm).**

**Table S2 Tri-exponential decay time constants of time-resolved transient PL acquired from POP-DT and POP-DF**

| Sample | $\tau_1$/ns | $\tau_2$/ns | $\tau_3$/ns | $Rel_1$% | $Rel_2$% | $Rel_3$% | τ/ns |
|---|---|---|---|---|---|---|---|
| POP-DF | 0.1506 | 0.6306 | 2.0149 | 39.66 | 49.79 | 10.55 | 0.59 |
| POP-DT | 0.1346 | 0.5496 | 1.8471 | 52.68 | 42.64 | 4.68 | 0.39 |

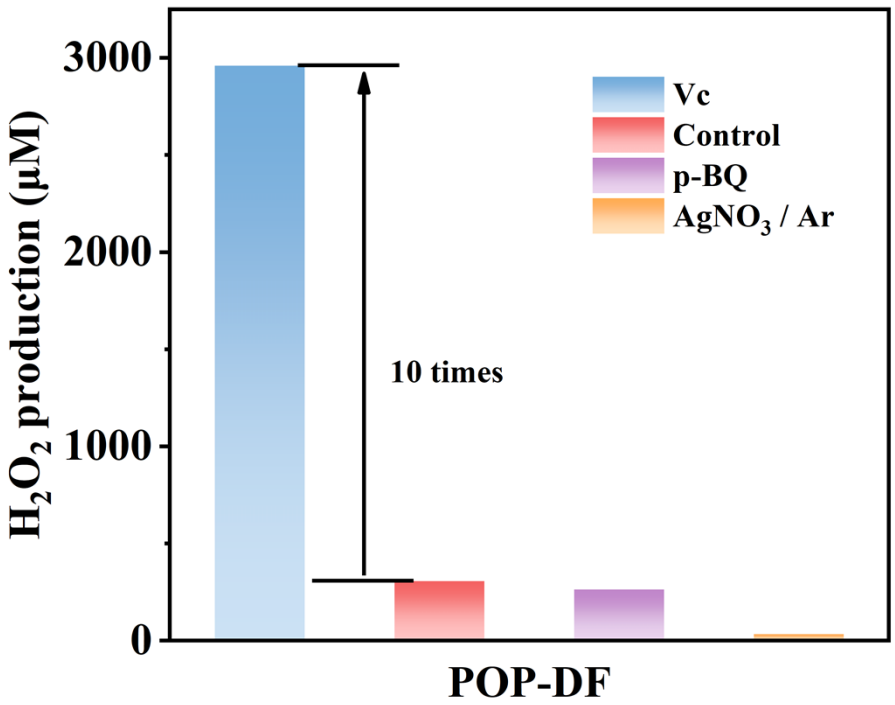


**Figure S12. Comparison of $H_2O_2$ production by POP-DT under the different conditions over one hour: Control, VC (5 mM), BQ (4 mM) and $AgNO_3$ (2 mM)/Ar.**

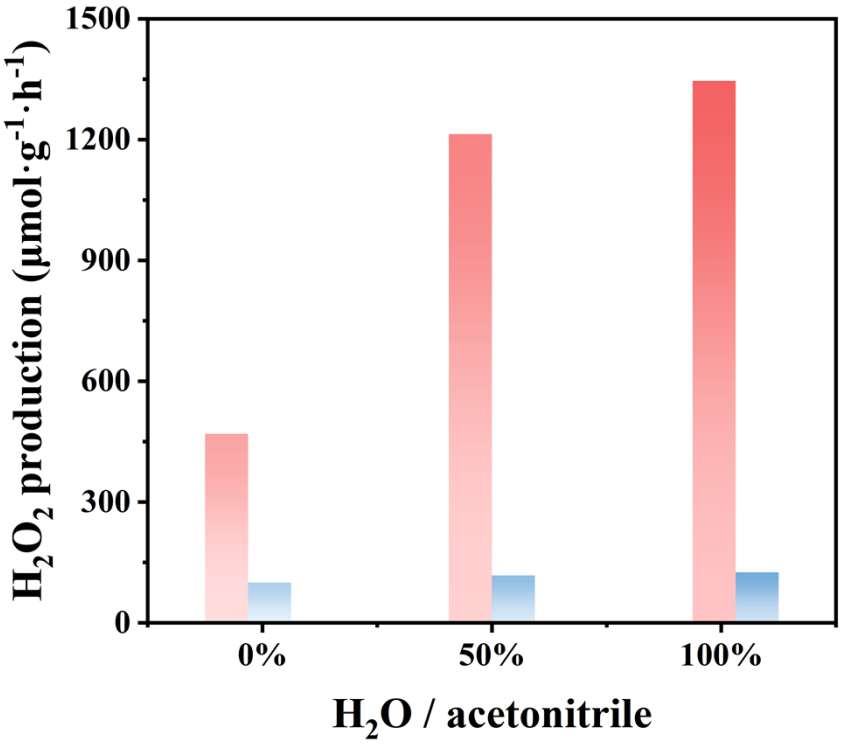


**Figure S13. Hydrogen peroxide generation efficiency under different ratios of water and acetonitrile mixed solutions.**

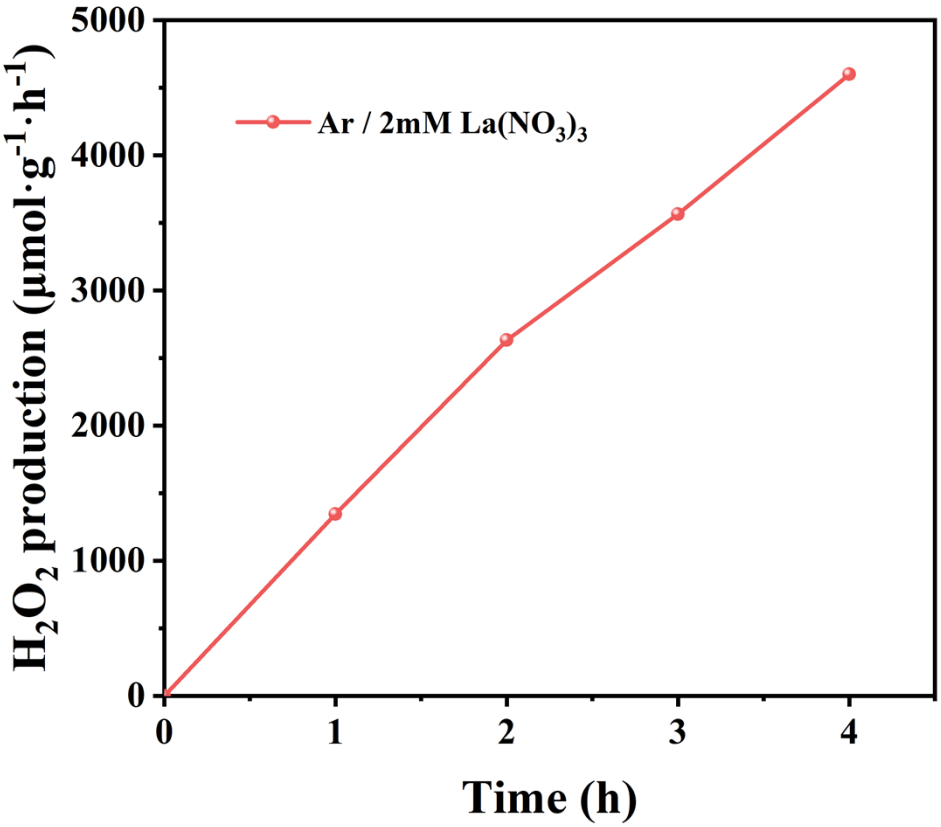


**Figure S14**. **Hydrogen peroxide generation yield in mixed solution of water (10 mL) and acetonitrile (10 mL) with (2 mM $La(NO_3)_3$ solution with Argon atmosphere, 10 mg photocatalyst in 20 mL solvent system, λ > 420 nm 300 W Xe lamp).**

We added two experimental pairs to further confirm that the hole of POP-DT produces hydrogen peroxide [9,10]: Firstly, we tested the reaction system with different proportions of water and acetonitrile under the conditions of Ar saturation and 2mM $La(NO_3)_3$. The yield of hydrogen peroxide in POPs. According to the experimental results (**Figure S13**), we know that with the water ratio increases, POP-DT exhibits gradually increasing hydrogen peroxide yield, while the comparative sample POP-DF is almost constant. Immediately, we further tested the accumulation rate of hydrogen peroxide production of POP-DT in 2mM $La(NO_3)_3$. and 50% water under continuous argon flow (**Figure S14**). The results showed that hydrogen peroxide continued to grow within four hours. Based on the above experimental results, we confirmed that the photocatalyst POP-DT can oxidize water at the hole end to produce hydrogen peroxide.

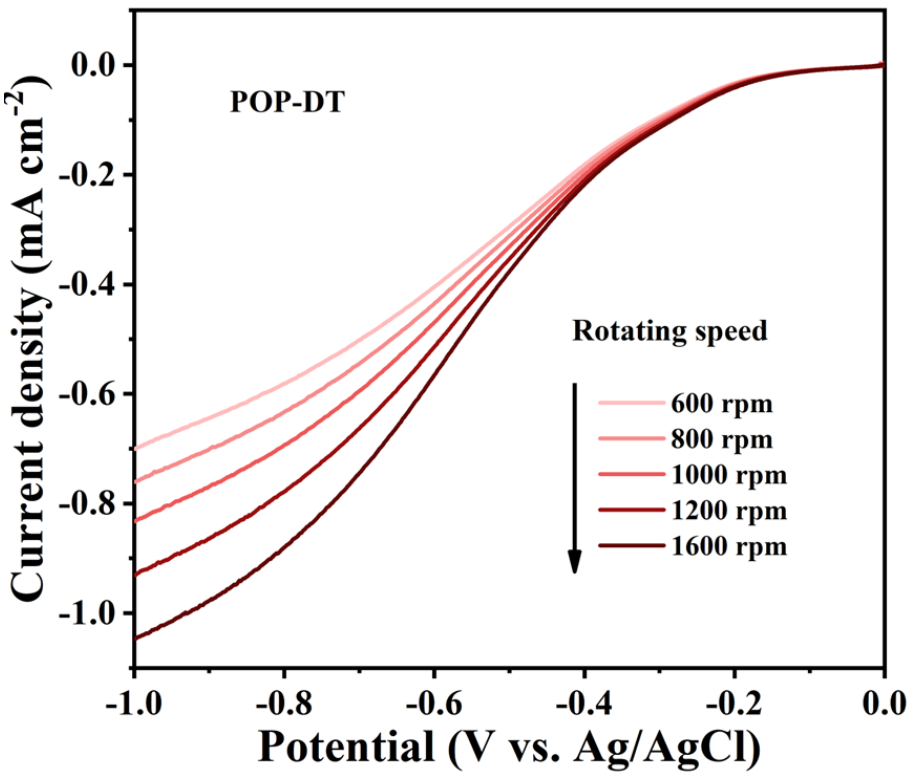


**Figure S15. Linear-sweep RDE voltammograms of POP-DT**.

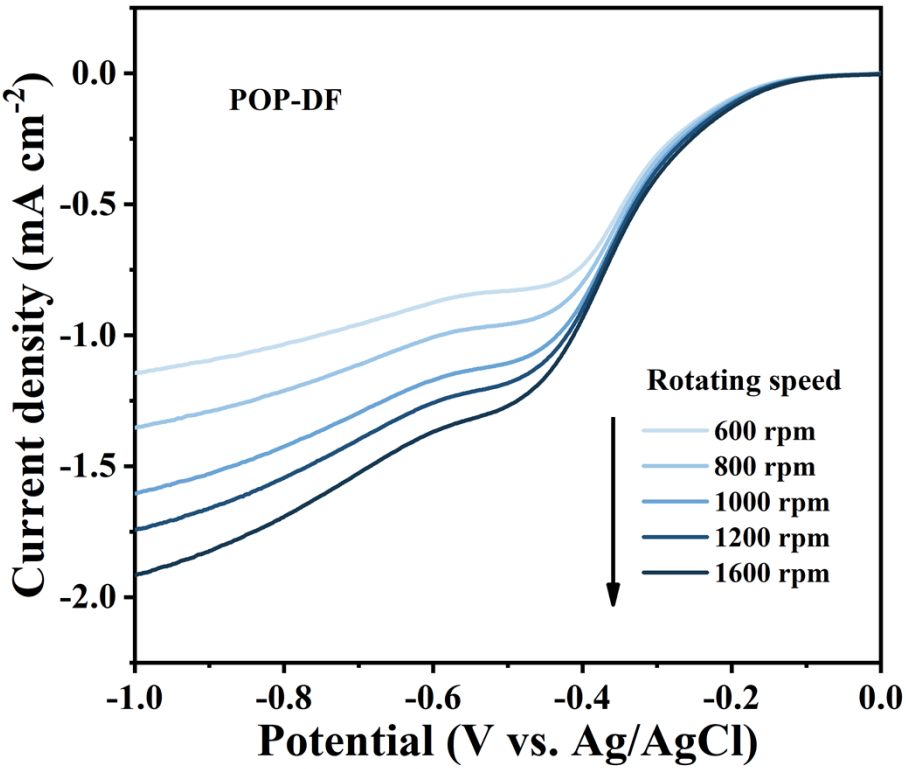


**Figure S16. Linear-sweep RDE voltammograms of POP-DF**.

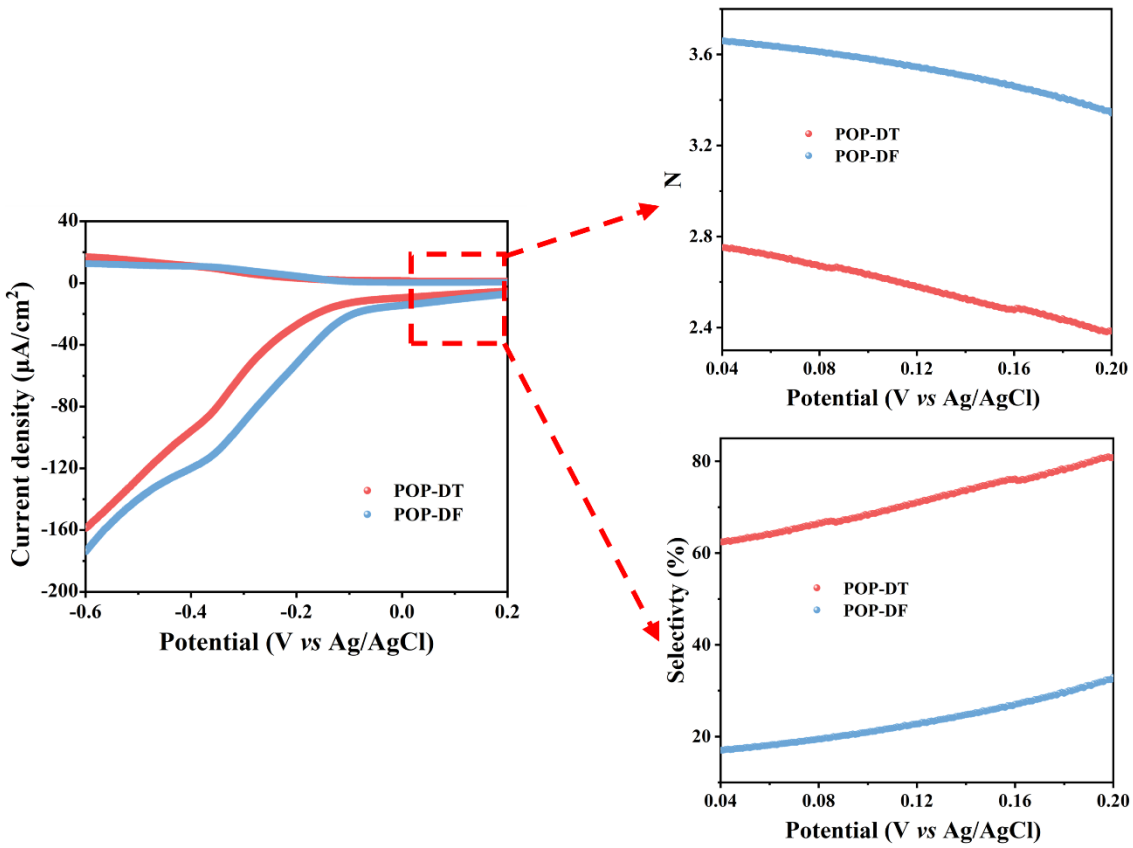


**Figure S17. Linear-sweep RRDE voltammograms of POPs measured at 1600 rmp rotating speeds under 10 mV $s^{-1}$ in $O_2$-saturated 0.5 M phosphate buffer solution and corresponding number of transferred electrons and selectivity of POPs.**

According to the experimental results, POP-DT has a higher reduction current compared to POP-DF, indicating a higher ability to reduce oxygen to hydrogen peroxide. The result showed that the two-electron selectivity of the photocatalyst POP-DT reached about 70% (Selectivity POP-DF = 30%), and the transferred electrons number is around 2.6 (NPOP-DF = 3.4). From this, we once again confirmed that among two photocatalysts mentioned in the article, POP-DT has more excellent two-electron oxygen reduction selectivity, and at the same time verified its stronger oxygen reduction efficiency to produce hydrogen peroxide.

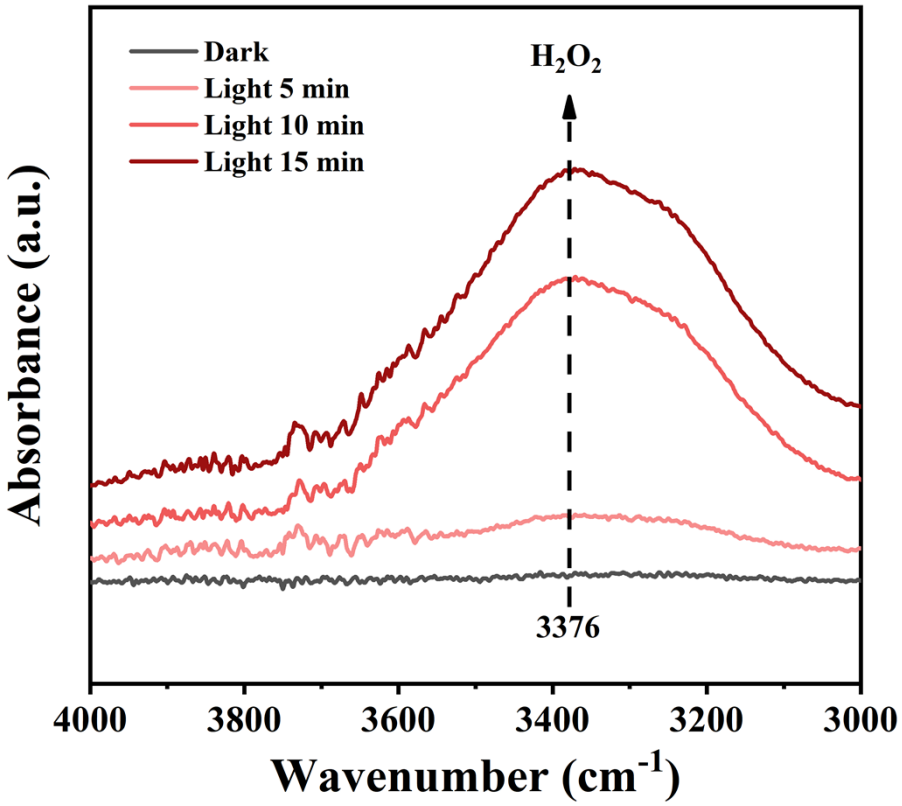


**Figure S18**. ***In situ*** **DRIFT spectra of POP-DT recorded during photocatalytic $H_2O_2$ evolution**.

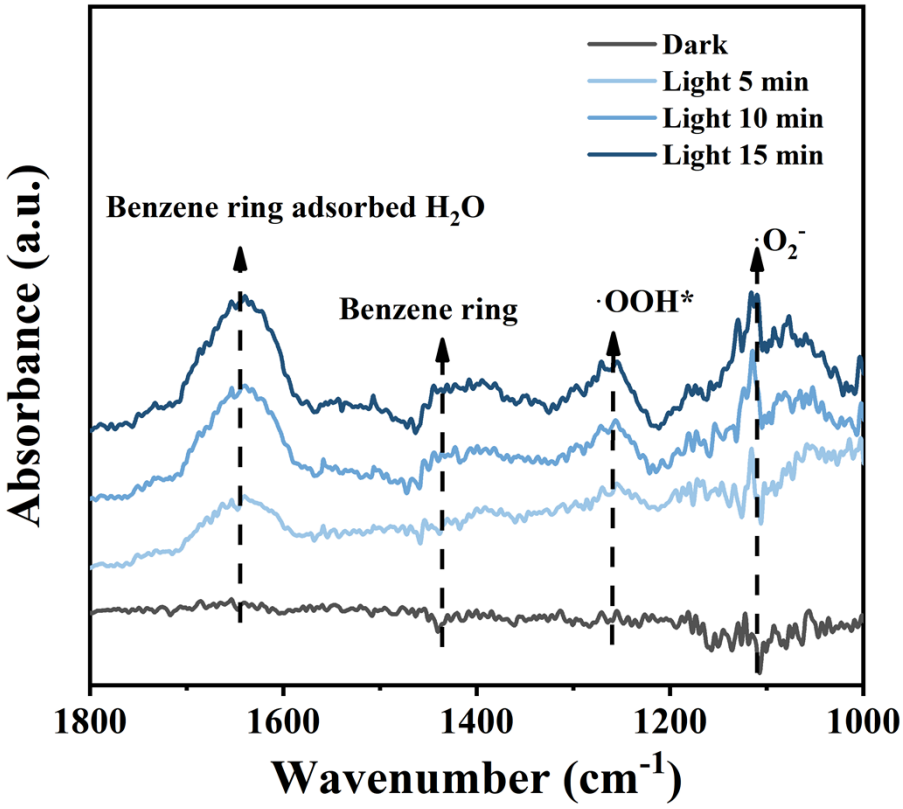


**Figure S19**. ***In situ*** **DRIFT spectra of POP-DF recorded during photocatalytic $H_2O_2$ evolution**.

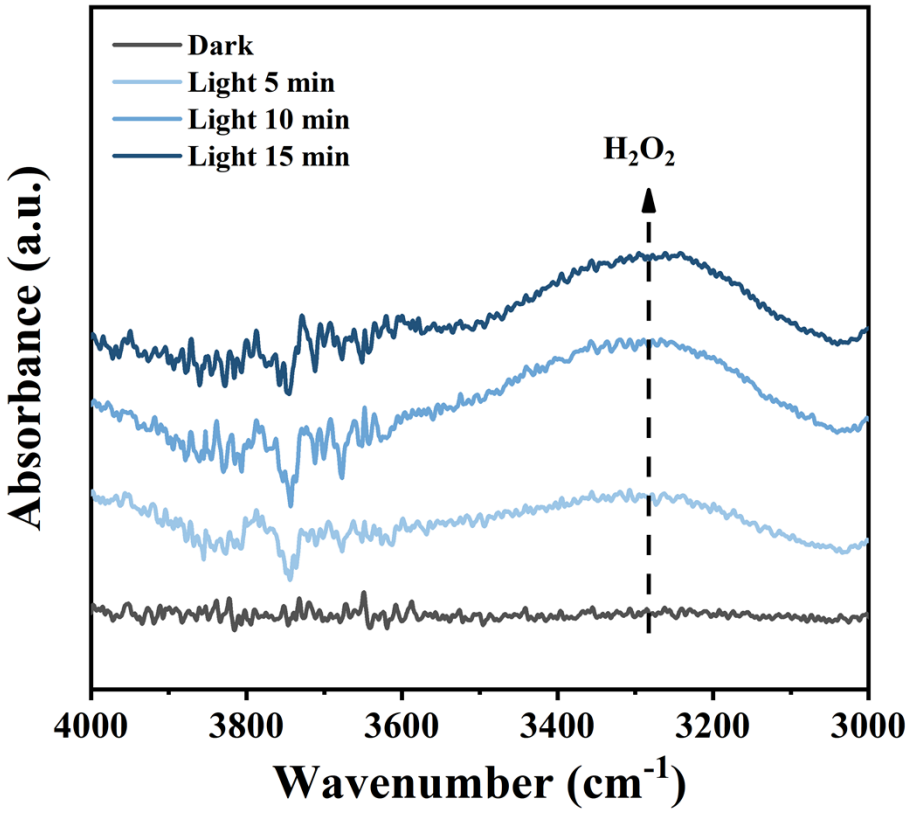


**Figure S20. In situ DRIFT spectra of POP-DF recorded during photocatalytic $H_2O_2$ evolution.**

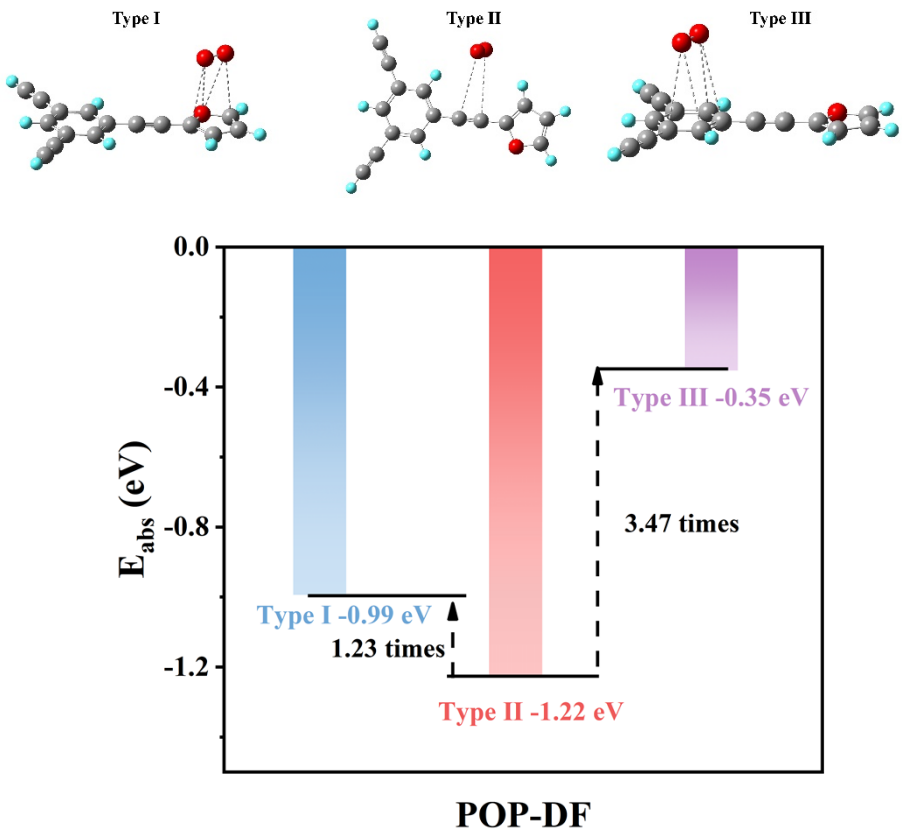


**Figure S21. The adsorption energy of $O_2$ at different sites for POP-DF.**

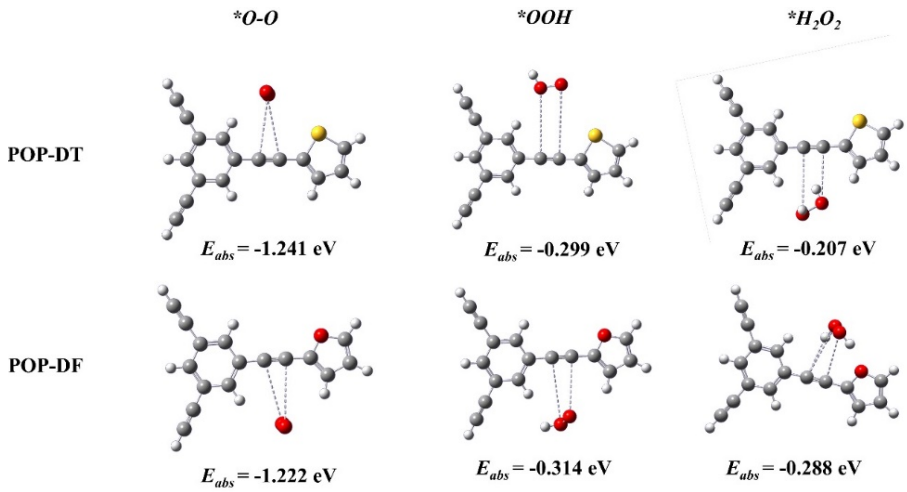


**Figure S22. The adsorption energy of *O-O, *OOH and *$H_2O_2$ at different alkynyl sites of POPs.**

In the process of converting oxygen into hydrogen peroxide, the acetylene position of POPs can achieve the adsorption of *O-O, *OOH, and *$H_2O_2$. Among them, POP-DT can better absorb oxygen. At the same time, both of them are good for *OOH. have almost the same adsorption capacity. In particular, POP-DF has stronger adsorption of *$H_2O_2$, which reduces the hydrogen peroxide in the aqueous solution. At the same time, the slow desorption of the hydrogen peroxide product further affects the next step. The adsorption of oxygen on acetylene sites further reduces the photocatalytic efficiency.

[1]R. Peverati; D. G. Truhlar. *Journal of Chemical Theory and Computation* 2012, *8*, 2310-2319.

[2]R. Peverati; D. G. Truhlar. *Physical Chemistry Chemical Physics* 2012, *14*, 13171-13174.

[3]A. Austin; G. A. Petersson; M. J. Frisch; F. J. Dobek; G. Scalmani; K. Throssell. *Journal of Chemical Theory and Computation* 2012, *8*, 4989-5007.

[4]R. Peverati; D. G. Truhlar, M11-L. *Journal of Physical Chemistry Letters* 2012, *3*, 117-124.

[5]F. Neese, The ORCA program system. Science 2012, *2*, 73-78.

[6]S. Grimme; S. Ehrlich; L. Goerigk. *Journal of Computational Chemistry* 2011, *32*, 1456-1465.

[7]S. Grimme; J. Antony; S. Ehrlich; H. Krieg. *Journal of Chemical Physics* 2010, *132*, 154104.

[8]Y. Zhao; N. E. Schultz; D. G. Truhlar. *Journal of Chemical Physics* 2005, *123*, 161103.

[9]C. C. Chu; Z. Chen; D. C. Yao; X. R. Liu; M. J. Cai; S. Mao. *Angewandte Chemie-International Edition* **2024**, *23*, e202317214.

[10]X. Zhang; S. Cheng; C. Chen; X. Wen; J. Miao; B. Zhou; M. Long; L. Zhang. *Nature Communications* **2024**, *15*, 2649.